Cluster Shape Anisotropy in Irreversibly Aggregating Particulate Systems

D. Fry,* A. Mohammad, A. Chakrabarti, and C. M. Sorensen

Department of Physics, Cardwell Hall, Kansas State University, Manhattan, Kansas 66506-2601

Received March 3, 2004. In Final Form: June 4, 2004

The results for cluster shape anisotropy over a broad range (10^{-3}−10^{-1}) of monomer volume fractions, f_v values, are presented for both two- (2d) and three-dimensional (3d) simulations of diffusion-limited (DLCA), ballistic-limited (BLCA), and reaction-limited (RLCA) cluster−cluster aggregation classes. We find that all three aggregation classes have different dilute-limit shape anisotropies, with the diffusion-limited model having the largest value of anisotropy and the reaction-limited model having the smallest. The simulation result for the cluster shape anisotropy for each of the three aggregation classes is slightly less than the corresponding prediction of the hierarchial model. In addition, we find excellent agreement between the 2d DLCA simulation results and experimental measurements of shape anisotropy. At late times, shape anisotropy decreases from the dilute-limit value.

1. Introduction

Unstable particulate systems, such as aerosols and colloids, form fractal aggregates by irreversible aggregation. These are found in a wide class of systems in both our technology and Nature[1] including biological gels, aerogel and xerogel lightweight thermally insulating materials, catalyst supports, paint processing, and numerous foods. More recent work on aggregation processes includes the synthesis of soft microgel particles,[2] chemical pulping,[3] superaggregate formation in soot,[4] selective aggregation of binary colloids,[5,6] and fabrication of novel composite materials.[7−9] It is well-known that in the absence of coalescence the resulting aggregates are structurally self-similar fractals described by the mass fractal dimension, D_f. In addition to the mass fractal dimension, a detailed understanding of aggregate shape anisotropy is important, as many fundamental properties of systems composed of these aggregates depend on their shape. For instance, transport, flow, and mechanical properties such as viscosity and elasticity may show anisotropic features if the clusters themselves are anisotropic.[10] Optical properties may also depend on shape anisotropy, since the dielectric constant may be different along different spatial directions, leading to birefringence. Although structural studies have produced a wealth of information, there are relatively few known studies addressing cluster shape.

From an experimental perspective, cluster shape is not an easily determined quantity. Both radiative and neutron scattering are frequently used tools for studying structural properties which are revealed through the scattered intensity. Often, aggregates are dispersed throughout externally field free isotropic media, and as a result, the mean aggregate orientation is isotropic. The scattered intensity then represents a spherical average over all possible aggregate orientations, eliminating the details of shape. Previous work has attempted to extract information on aggregate shape from light scattering measurements by spherical harmonic expansion of the structure factor.[11] However, only a relative measure for aggregates grown by different methods was given. Several early studies utilized electron micrograph techniques and computer simulation to investigate the shape of carbonaceous soot ("carbon black") clusters. Results were limited simply because the 3d aggregates were projected into 2d images and simulation was confined to linear trajectory particle−cluster aggregation models.[12,13] The latter is analogous to diffusion-limited particle−cluster aggregation (DLA),[14] used extensively to model dendritic growth and some structures grown by deposition but not valid for numerous colloidal and aerocolloidal aggregate systems found in nature.

The majority of previous simulation studies of cluster shape used the hierarchial model (HM).[15,16] This model utilizes renormalization groups and scaling concepts for studying various properties of aggregates. Clusters produced by the HM have mass fractal dimensions of $D_f = 1.42$ for 2d diffusion-limited growth,[15] in excellent agreement with experiment, and also reproduce the well-known "stringy" appearance of clusters seen in several different aggregating systems.[17,18] Quantitatively, however, the

* Corresponding author. Present address: Physics Division, National Institute of Standards and Technology, Gaithersburg, MD 20899. E-mail: dan.fry@nist.gov.

(1) Brinker, C. J.; Scherer, G. W. *Sol Gel Science: The Physics and Chemistry of Sol−Gel Processing*; Academic: Boston, MA, 1990.
(2) Fernandez-Nieves, A.; Fernandez-Barbero, M.; Vincent, B.; de las Nieves, F. J. *Langmuir* **2001**, *17*, 1841.
(3) Norgren, M.; Edlund, H.; Wagberg, L. *Langmuir* **2002**, *18*, 2859.
(4) Sorensen, C. M.; Kim, W.; Fry, D.; Shi, D.; Chakrabarti, A. *Langmuir* **2003**, *19*, 7560.
(5) Hiddessen, A. L.; Rodgers, S. D.; Weitz, D. A.; Hammer, D. A. *Langmuir* **2000**, *16*, 9744.
(6) Pierce, F.; Chakrabarti, A.; Fry, D.; Sorensen, C. M. *Langmuir* **2004**, *20*, 2498.
(7) Hanus, L. H.; Sooklal, K.; Murphy, C. J.; Ploehn, H. J. *Langmuir* **2000**, *16*, 2621.
(8) Kim, A.; Berg, J. C. *Langmuir* **2000**, *16*, 2101.
(9) Ehrburger-Dolle, F.; Hindermann-Bischoff, M.; Livet, F.; Bley, F.; Rochas, C.; Geissler, E *Langmuir* **2001**, *17*, 329.
(10) Petrie, C. J. S. *Rheology*; Pitman: London, 1979.
(11) Lindsay, H. M.; Klein, R.; Weitz, D. A.; Lin, M. Y.; Meakin, P. *Phys. Rev. A* **1989**, *39*, 3112.
(12) Sutherland, D. N.; Goodarz-Nia, I. *Chem. Eng. Sci.* **1971**, *26*, 2071.
(13) Ravey, J. C. *J. Colloid Interface Sci.* **1975**, *50*, 545.
(14) Witten, T. A., Jr.; Sander, L. M. *Phys. Rev. Lett.* **1981**, *47*, 1400.
(15) Botet, R.; Jullien, R.; Kolb, M. *J. Phys. A* **1984**, *17*, L75.
(16) Botet, R.; Jullien, R. *J. Phys. A* **1986**, *19*, L907.
(17) Vicsek, T. *Fractal Growth Phenomena*; World Scientific: River Edge, NJ, 1992.
(18) Robinson, D. J.; Earnshaw, J. C. *Phys. Rev. A* **1992**, *46*, 2045.

10.1021/la0494369 CCC: $27.50
Published on Web 08/06/2004

degree of "stringyness", or the magnitude of shape anisotropy in 2d is in disagreement with experiment.[18] Furthermore, the HM is limited to aggregation for dilute systems and thus cannot address cluster properties such as shape for systems that evolve from dilute to dense, common for aggregating fractal clusters.

Although complex, most of the aforementioned real systems show a remarkable likeness to predictions of well-known nonequilibrium aggregation models.[2,3,9,12,13] Fortuitous for us, it allows for simulation of large systems at very little computational expense. The aim of this paper is thus to investigate aggregate shape via 2d and 3d large-scale off-lattice Monte Carlo simulations of diffusion-limited, ballistic-limited, and reaction-limited cluster−cluster aggregation. We compare our 2d simulation results with experiments on the 2d aggregation of polystyrene spheres and find better agreement than the hierarchial model. In addition, we comment, within the limited late time accuracy of our data, on changes in cluster shape as the system evolves to a dense state.

2. Characterizing Cluster Shape

The radius of gyration, R_g, of a cluster is a measure of its *overall* size. It is a root-mean-square (rms) radius weighted by the cluster mass density, $\rho(\vec{r})$, expressed as

$$R_g^2 = \frac{\int r^2 \rho(\vec{r})\, d\vec{r}}{\int \rho(\vec{r})\, d\vec{r}} \tag{1}$$

where r is the radial distance measured from the cluster center of mass and the denominator is equal to the total cluster mass, M. It is well-known[19] that the mass density is well-represented by a power law in radial distance; that is, $\rho(\vec{r}) = \rho_0 r^{D_f - d}$, where d is the space dimension. Cluster mass then scales with geometric size as $M \propto R_g^{D_f}$. However, this measure supplies only an orientationally averaged description of a cluster and provides no details of its actual shape.

The shape of any object can be characterized by its symmetric moment of inertia tensor, $\mathbf{T}_I$, with components

$$T_{ij} = \int \rho(\vec{r}) q_i q_j\, d\vec{r} \quad \text{for} \quad i, j = 1, \ldots, d,\ i \neq j$$

$$T_{ii} = \int \rho(\vec{r})(r^2 - q_i^2)\, d\vec{r} + I_m \quad \text{for} \quad i = 1, \ldots, d \tag{2}$$

where $q_i = x$, y, and z for $i = 1$, 2, and 3, respectively. Although a small effect at large cluster sizes, we have included the moment of inertia of individual monomeric units comprising the cluster, I_m. These monomers are treated as circles (spheres) in 2d (3d). Diagonalizing and dividing by the total cluster mass, M, gives the squares of *principle* radii of gyration, R_i^2, for $i = 1, \ldots, d$. Considering that the trace of $\mathbf{T}_I$ is invariant, the shape and overall size are related by

$$R_g^2 = \frac{1}{2}[R_1^2 + R_2^2 + R_3^2] \tag{3}$$

We characterize cluster shape by looking at the mean shape anisotropy for the ensemble of clusters. Analogous to previous work,[12,16,20,21] the mean anisotropy is defined in terms of ratios of the squares of the principle radii of gyration

$$\langle A_{ij} \rangle = \left\langle \frac{R_i^2}{R_j^2} \right\rangle \quad \text{for} \quad i \neq j,\ R_i > R_j \tag{4}$$

where the brackets indicate an ensemble average[22] and $i, j = 1, \ldots, d$.

An alternate way to cast the anisotropy, which lends itself as a measure of the geometric extent of a cluster, is in terms of an equivalent ellipsoid. This treats the mass distribution as homogeneous but utilizes the principle radii of gyration. The principle radii of gyration of a 3d ellipsoid with axes lengths $d_i = a$, b, and c for $i = 1$, 2, and 3, respectively, are

$$R_i^2 = \frac{2}{5}(d_j^2 + d_k^2) \quad \text{for} \quad i \neq j \neq k \tag{5}$$

where $i, j, k = 1, 2, 3$. Solving for d_i yields

$$d_i = \left[\frac{5}{2}((1 - 2\delta_{i1})R_1^2 + (1 - 2\delta_{i2})R_2^2 + (1 - 2\delta_{i3})R_3^2)\right]^{1/2} \tag{6}$$

where δ_{ij} is the Kronecker delta and $i = 1$, 2, and 3 corresponds to axes a, b, c, respectively, ordered from smallest to largest. A full discussion regarding the use of $\mathbf{T}_I$ and the inertia equivalent ellipsoid, as well as the relationship between the two, is left for the appendix.

3. Simulation Method

In the absence of external forces, aggregation of particulate dispersions is governed almost entirely by the relative strengths of attractive and repulsive interactions between the dispersed particles.[23] If the repulsion is entirely suppressed and the attractive potential is negligible except at particle contact, the aggregation rate is limited only by the particle dynamics, which in general is diffusive (random walk) or ballistic (linear trajectory, important in rarified gases). Upon colliding, clusters "stick" together with unit probability P_{stick}. If there is some degree of repulsion, not all collisions result in clusters getting close enough to stick together and $P_{stick} < 1$. Typically, the repulsive barrier, E_b, between colloidal particles is ≈50−100 meV.[23] The probability then, at room temperature, that two particles stick together is $P_{stick} \approx \exp(-E_b/k_B T) \approx 10^{-3}$. With this in mind, many physical systems can be separated into essentially three aggregation classes: diffusion-limited cluster−cluster aggregation (DLCA), ballistic-limited cluster−cluster aggregation (BLCA), and reaction-limited cluster−cluster aggregation (RLCA). We model these three aggregation classes following these criteria:

(1) DLCA: diffusive cluster motion, $P_{stick} = 1$.

(2) BLCA: ballistic (linear trajectory) cluster motion, $P_{stick} = 1$.

(3) RLCA: diffusive cluster motion, $P_{stick} = 10^{-3}$.

In all models presented, we assume that the attractive potential is infinite at particle contact, that is, the clusters stick together irreversibly upon colliding.

(19) Julien, R.; Botet, R. *Aggregation and Fractal Aggregates*; World Scientific: River Edge, NJ, 1987.

(20) Hentschel, H. G. E. In *Kinetics of Aggregation and Gelation*, Proceedings of the International Topical Conference on Kinetics of Aggregation and Gelation, Athens, GA, Apr 2−4, 1984; Family, F., Landau, D., Eds.; Elsevier Science Publishers B.V.: Amsterdam, The Netherlands, 1984.

(21) Family, F.; Vicsek, T. *Phys. Rev. Lett.* **1985**, *55*, 641.

(22) We differ from previous work in how the anisotropy is *averaged*. Past work has used $\langle\ \rangle/\langle\ \rangle$, as opposed to our definition which is $\langle - \rangle$.

(23) Hunter, R. *Foundations of Colloid Science*; Clarendon Press: Oxford, U.K., 1987.

Utilizing the above modeling scheme, we have performed large-scale off-lattice Monte Carlo (OLMC) simulations in a box, allowing us to track the morphology from the dilute to dense aggregation regimes over 3 orders of magnitude of the monomer volume fraction, f_v. The simulation is identical to that used in previous work.[24] We begin by randomly placing off-lattice N_m monomers in a cubic box of side length L. The simulation then proceeds by first randomly picking, with the probability N_c^{-1}, a cluster of size N (number of monomers per cluster), where N_c is the number of clusters at time t. A cluster is moved, with the probability N^{-1/D_f}, one monomer diameter either in a randomly chosen direction for the DLCA and RLCA classes or with a straight line trajectory for the BLCA class. D_f is the well-known dilute-limit mass fractal dimension of a cluster in each respective aggregation class. Each time a cluster is picked, the time, measured in Monte Carlo steps per cluster, is incremented by N_c^{-1} regardless of whether the cluster has moved. If two clusters collide, and hence aggregate, the motion is adjusted in order to correct for any overlap between particles.

Because $D_f < d$, the ratio of nearest-neighbor separation, R_{nn}, to the radius of gyration, R_g, decreases with time as $R_{nn}/R_g \propto t^{-z(d-D_f)/dD_f}$, where the kinetic exponent z is >0.[24] Consequently, the aggregates become increasingly crowded as the system evolves. This is true for all three aggregation classes. The degree of cluster crowding is measured by calculation of the cluster volume fraction, f_v^c, available in the system at any given time, where

$$f_v^c(t) = \frac{4\pi}{3L^3}\left(\frac{D_f + 2}{D_f}\right)^{3/2} \sum_{i=1}^{N_{c(t)}} R_{g,i}^{\ 3} \qquad (7)$$

This is an approximate measure, since it assumes that the clusters are spherical in shape, contrary to what is found. However, as will be shown, since the shape is more spherical than "stick-like", it is still useful as a measure of the degree of crowdedness.

Throughout the results to follow, "early" and "late" time corresponds directly to $f_v^c(t) \ll 1$ and $f_v^c(t) \simeq 1$, respectively. As will be shown, f_v^c is a "good" parameter for characterizing cluster shape, and we choose it over time. The cluster number, size distribution along with its moments, free volume, and radius of gyration are monitored throughout the simulation. The actual gel point is determined by looking for the first system-spanning cluster and is denoted in the figures by vertical arrows.

We calculate, assuming a monodisperse size distribution, the radius of gyration at which a cluster is just touching its neighbors, i.e., the *ideal* gel point radius of gyration, $R_{g,G}$, by

$$R_{g,G} = a\left[k_0^{-1}\left(\frac{D_f + 2}{D_f}\right)^{3/2} f_v\right]^{-1/(3-D_f)} \qquad (8)$$

where a is the monomer radius and k_0 a constant of order unity.[25] Note the dependence on the monomer volume fraction, f_v. Assuming fractal clusters with $N \sim R_g^{D_f}$, we estimate the number of monomers per cluster at the ideal gel point, N_G. Finally, taking $N_G \simeq N_m/N_{c,G}$ with the number of clusters at the ideal gel point $N_{c,G} \sim 100$, we arrive at an estimate for N_m. All OLMC simulations presented here have been done at system sizes ranging from 800 000 to 3×10^6 monomers and box sizes of $L = (162-580)d_m$, where $d_m = 2a$ is the monomer diameter. To rule out finite size effects of the box, we have performed simulations at $f_v = 0.005$ for box sizes of $L = 50$, 100, 200, and 540. The dilute-limit shape anisotropy showed no difference with box size beyond statistical fluctuation. However, the lower box sizes, for the reasons listed above, never gelled.

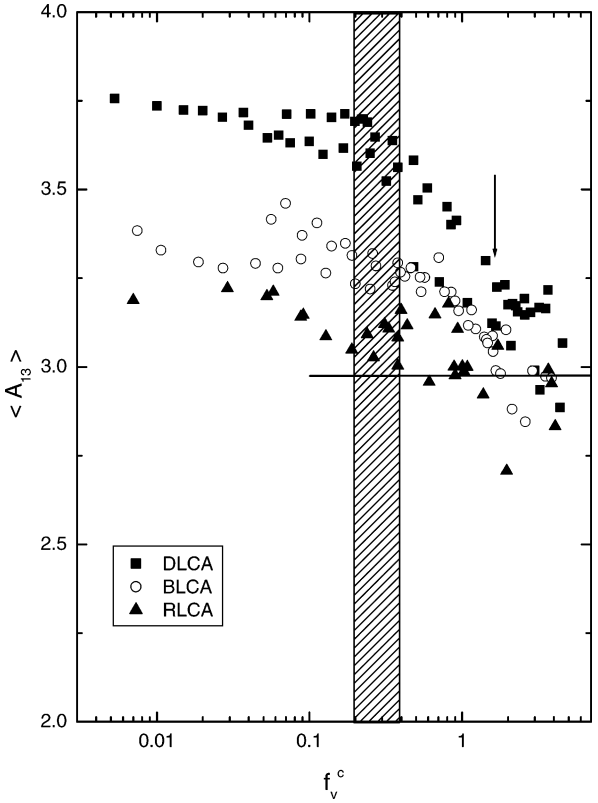

Figure 1. Anisotropy $\langle A_{13}\rangle$ as a function of the cluster volume fraction for the DLCA, BLCA, and RLCA models. Since $\langle A_{13}\rangle$ is independent of f_v, combined results for all $f_v = 0.001$, 0.005, 0.01, and 0.1 for each aggregation class are shown with the same symbol. The shade region marks the 3d percolation thresholds for the cubic, fcc, and bcc lattices, continuum percolation, and percolation of randomly placed ellipsoids. The presence of the first system-spanning cluster, or percolation point, is designated by the vertical arrow. This point is roughly the same for each class. As a guide to the eye, the anisotropy for the 3d site percolation clusters is shown and designated by the solid horizontal line.

Average shape anisotropy is determined in the following manner. At a particular f_v^c value (and time), we calculate the shape anisotropy in terms of eqs 4 and 6 for each cluster in the ensemble for which $N \geq 5$ monomers per cluster. We then average over the entire ensemble of $N_c(t)$ clusters, where 500 000 $\geq N_c(t) \geq$ 100 depending on the degree to which the system has aggregated. This procedure is performed for five statistically independent runs for each monomer volume fraction and aggregation class. The large f_v^c (late time) regime near the gel point will have more statistical fluctuation about the mean because there are fewer clusters present.

4. Results and Discussion

Shape anisotropy results in terms of $\langle A_{ij}\rangle$ (eq 4) are shown in Figures 1 and 2, and the ratios of equivalent ellipsoid axes are shown in Figures 3 and 4, both as a function of the cluster volume fraction for the DLCA, BLCA, and RLCA models. For each of the three aggregation classes,

(24) Fry, D.; Sintes, T.; Chakrabarti, A.; Sorensen, C. M. *Phys. Rev. Lett.* **2002**, *89*, 148301-1.
(25) Sorensen, C. M.; Roberts, G. *J. Colloid Interface Sci.* **1997**, *186*, 447.

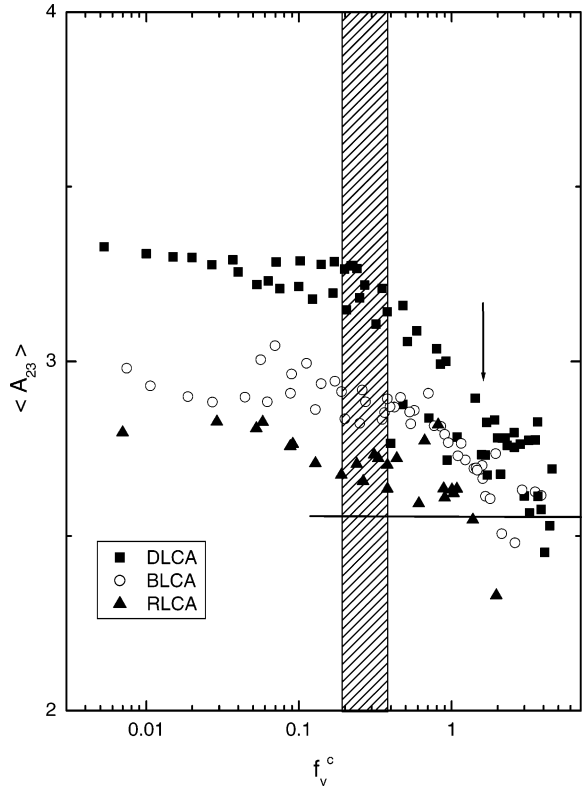

Figure 2. Same as in Figure 1 except anisotropy $\langle A_{23} \rangle$ is plotted here.

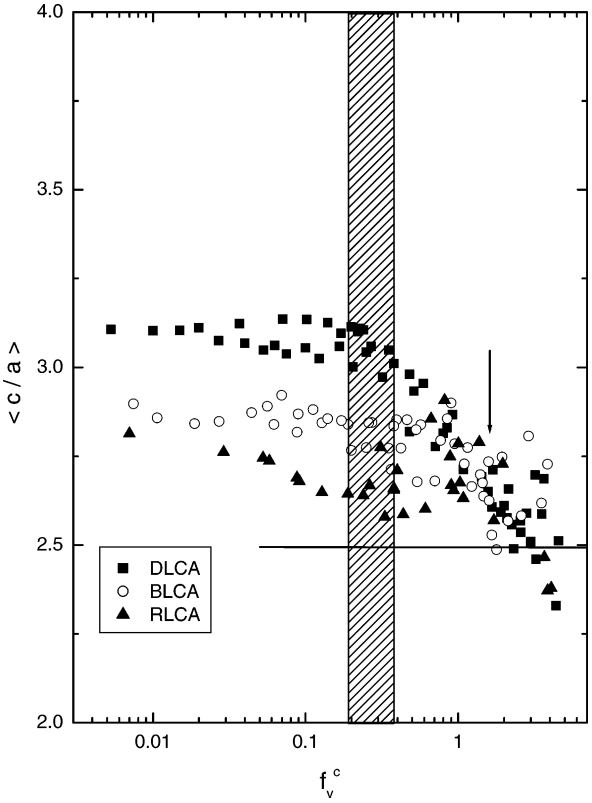

Figure 3. Same as in Figure 1 except anisotropy $\langle c/a \rangle$ is plotted here.

cluster shape anisotropy is constant when the system is dilute. This is in agreement with a previous model.[26] However, this dilute-limit anisotropy is different for

(26) Sorensen, C. M.; Oh, C. *Phys. Rev. E* **1998**, *58*, 7545.

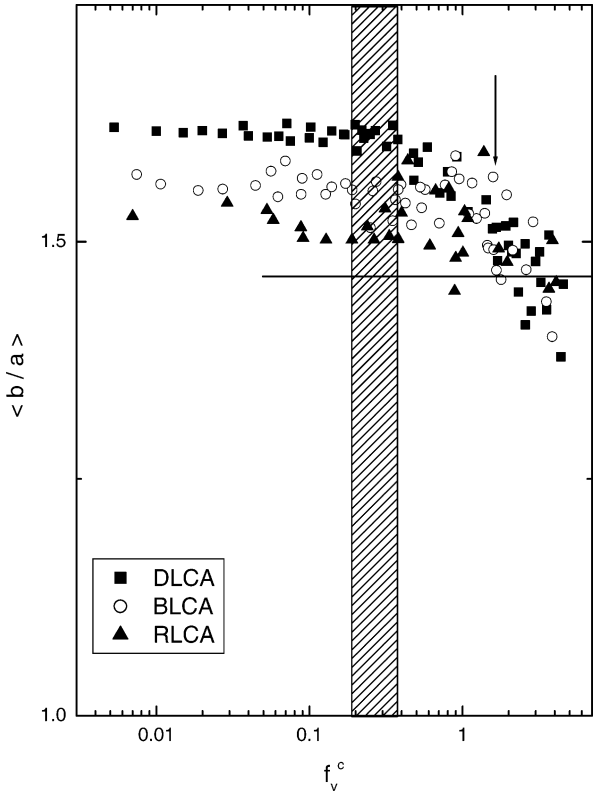

Figure 4. Same as in Figure 1 except anisotropy $\langle b/a \rangle$ is plotted here.

different aggregation classes. Although previous work with the HM on cluster shape in 2d has seen similar trends,[16] this has never been investigated with more realistic off-lattice cluster−cluster aggregation models. Note that once the system has evolved to a critical cluster volume fraction (most emphasized for the DLCA class), the anisotropy starts to decrease.

In what follows, we characterize the dilute-limit anisotropy in great detail. When appropriate, we compare our results with the hierarchial model, particle−cluster aggregation model, and with available (limited) experimental data.

4.1. Anisotropy When Dilute. As a test of our simulation method, we first determine the aggregate fractal dimension in the dilute limit by plotting the cluster mass, M, versus the radius of gyration, R_g, for the ensemble of aggregates. Results for all three models are in agreement with accepted values[27−30] and are listed in Table 1.

Now our goal is to understand aggregate shape when dilute. Using A_{ij} (Figures 1 and 2), clusters on average appear to resemble prolate spheroids, or are "cigar shaped", as shown by the relatively small difference between $\langle A_{13} \rangle$ and $\langle A_{23} \rangle$. Construction of the inertia equivalent ellipsoid (Figures 3 and 4) shows that the largest ellipsoid axis, c, is ∼3 times larger than the smallest axis, a. The ratios of axes, however, appear to be geometrically spaced, quite different from the spacing between $\langle A_{13} \rangle$ and $\langle A_{23} \rangle$.

Each aggregation class yields a different dilute-limit mean anisotropy, with the DLCA values being the largest

(27) Weitz, D. A.; Oliveria, M. *Phys. Rev. Lett.* **1984**, *52*, 1433.
(28) Hasmy, A.; Foret, M.; Pelous, J.; Jullien, R. *Phys. Rev. B* **1993**, *48*, 9345.
(29) Weitz, D. A.; Huang, J. S.; Lin, M. Y.; Sung, J. *Phys. Rev. Lett.* **1985**, *54*, 1416.
(30) Lin, M. Y.; Lindsay, H. M.; Weitz, D. A.; Ball, R. C.; Klein, R.; Meakin, P. M. *Phys. Rev. A* **1990**, *41*, 2005.

Table 1. Shape Anisotropy for the Dilute-Limit OLMC Model, HM, and PCA Model[a]

	OLMC			HM			PCA		
	DLCA	BLCA	RLCA	DLCA	BLCA	RLCA	DLA	BLA	RLA
P	2.0 ± 0.1	3.0 ± 0.25	12.1 ± 0.50	1	1	1			
D_f	1.75 ± 0.05	1.87 ± 0.05	2.19 ± 0.05	1.79 ± 0.02	1.92 ± 0.03	2.08 ± 0.10	2.41 ± 0.10	2.90 ± 0.05	3.01 ± 0.05
$\langle A_{13}\rangle$	3.70 ± 0.1	3.34 ± 0.1	3.18 ± 0.1	4.23 ± 0.2	3.97 ± 0.2	3.43 ± 0.2	1.32 ± 0.1	1.22 ± 0.1	1.37 ± 0.1
$\langle A_{23}\rangle$	3.29 ± 0.1	2.93 ± 0.1	2.80 ± 0.1	3.79 ± 0.2	3.55 ± 0.2	2.94 ± 0.2	1.15 ± 0.1	1.08 ± 0.1	1.25 ± 0.1
$\langle c/a\rangle$	3.09 ± 0.1	2.86 ± 0.1	2.74 ± 0.1	3.43 ± 0.2	3.27 ± 0.2	2.95 ± 0.1	1.35 ± 0.1	1.20 ± 0.1	1.36 ± 0.1
$\langle b/a\rangle$	1.61 ± 0.05	1.56 ± 0.05	1.51 ± 0.05	1.71 ± 0.1	1.62 ± 0.1	1.62 ± 0.1	1.21 ± 0.1	1.11 ± 0.1	1.13 ± 0.1

[a] $\langle A_{ij}\rangle$ is defined according to eq 4.

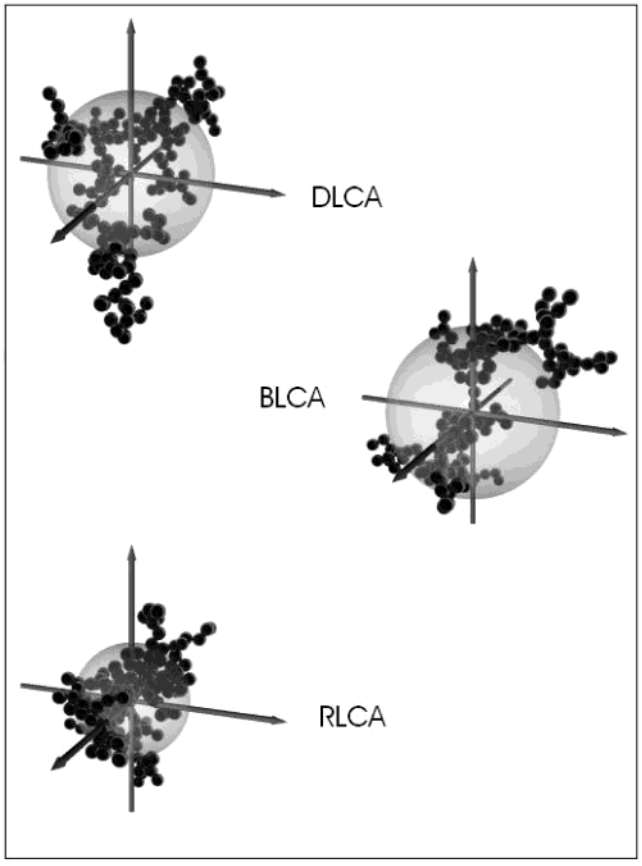

Figure 5. Stereographic view of sample clusters from each aggregation class. The semitranslucent sphere represents the measure of "overall" size and has a radius of R_g. The range of all the axes is the same for each aggregation class. The number of monomers per cluster is $N = 158$, 152, and 152 for DLCA, BLCA, and RLCA, respectively, thus allowing for direct comparison between the relative degree of compactness and stringy appearance.

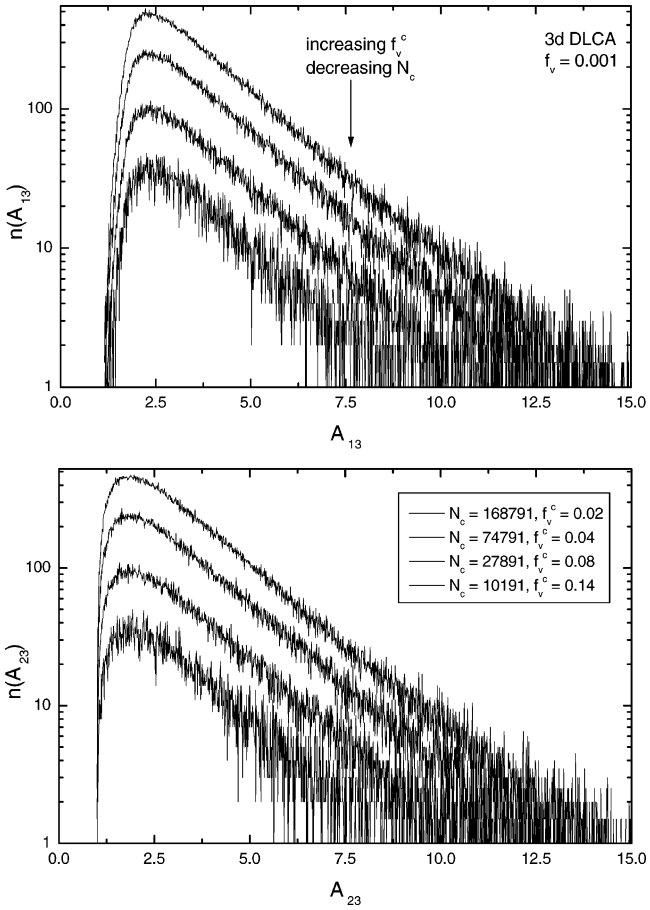

Figure 6. Distribution of A_{ij} for the 3d OLMC diffusion-limited model at an initial volume fraction of $f_v = 0.001$ for several f_v^c values (and times) in the dilute-limit regime. The legend applies to both parts of the figure.

and the RLCA values being the smallest. However, within each class, cluster shape is independent of the monomer volume fraction. Values for the dilute limit are summarized in Table 1. Figure 5 shows several sample stereographic views of the dilute-limit largest clusters from our off-lattice simulations for each aggregation class. Note the difference in compactness between DLCA and RLCA, represented by the difference in the respective fractal dimension, D_f (Table 1). The DLCA and BLCA aggregates look rather similar.

The distribution of A_{ij} at several times during aggregation for the dilute-limit DLCA simulation is shown in Figure 6. The results for BLCA and RLCA look similar. Both distributions are asymmetric with peak values of $A_{ij,p} \approx 2.3$ and 1.8 for $i, j = 1, 3$ and 2, 3, respectively. The distribution has a relatively long tail at early times out to values as large as ca. 15. The extent of the distribution with increasing A_{ij} decreases with increasing time. In the limit of large A_{ij}, the distribution appears exponential. Assuming $n(A_{ij}) \simeq \exp(-\mu_{ij}A_{ij})$ is valid at large A_{ij}, we have performed a linear regression on the DLCA curves in Figure 6, as well as those for BLCA and RLCA. When dilute (up to $f_v^c \simeq 0.14$), $\mu_{ij} \simeq 0.25$, 0.29, and 0.32 and constant for DLCA, BLCA, and RLCA, respectively. Currently, there is no known theoretical explanation for the shape of the distribution. We note, however, that information regarding the width of the distribution may help in understanding the rather complex rheological properties of systems composed of anisotropic shaped clusters. For instance, it has been observed that the shear viscosity in dense colloidal dispersions is larger for irregularly shaped particulates.[31]

4.1.1. Comparison with the Hierarchial and Particle–Cluster Aggregation Models and the Effects of Polydispersity. Because the hierarchial model (HM) is known to well-represent cluster structure in the dilute limit, we

(31) Tsai, S. C.; Botts, D.; Plouff, J. *J. Rheol.* **1992**, *36*, 1291.

chose to compare our more realistic off-lattice shape anisotropy results with the HM. Previous work with the HM[16] is essentially the only known detailed simulation study of cluster shape. However, the majority of previous results dealt with aggregation in 2d and measured shape slightly different than we do here.[22] For direct comparison with the OLMC model, we have carried out off-lattice hierarchial model (HM) simulations in 3d using our measure of shape anisotropy (eq 4).

The simulation begins by randomly choosing two clusters of size $N = 1$ monomers per cluster from an ensemble of N_m monomers. One monomer is held fixed at the center of the coordinate frame. The other is placed at radius R_c, always chosen to be several times the mean cluster perimeter radius, and allowed to undergo diffusive (diffusion-limited aggregation) or ballistic (ballistic-limited aggregation) motion until a collision is made with the stationary monomer. For the diffusion-limited and ballistic-limited cases, any collision results in clusters sticking together irreversibly. Reaction-limited aggregation was modeled in the same way as that described in section 3. This process is repeated between all monomers until the number of clusters has reduced to $N_m/2$ and thus completes the kth step of the algorithm. Note that each step results in a monodisperse cluster size distribution, a unique feature of the HM. Clusters were grown up to sizes of $N = 512$. At each kth step, the anisotropy was calculated for the ensemble of 2^{9-k} clusters. This was then averaged over 40 independent runs.

For $N > 16$, the shape anisotropy was found to be constant, independent of N, in agreement with previous results.[16] As a check, we used the measure of Botet et al.[16] and compared our off-lattice HM results with their on-lattice results. No difference in shape anisotropy was found. However, the HM results for all three aggregation classes (Table 1) using eq 4 seem to be systematically slightly larger than the OLMC results, which we discuss in the following.

The HM assumes that, in the scaling regime, collisions occur between clusters of equal size.[16,20] In our off-lattice Monte Carlo simulations, however, aggregation between "equal" sized clusters is not the *only* aggregation route. This is observed in Figure 7, where we histogram each binary collision event between clusters, of size N_1 and N_2 monomers per cluster, for the diffusion-limited class for successive time periods (increasing f_v^c) during aggregation. The results for BLCA and RLCA are similar. The distribution of binary collisions depends on the width of the cluster size distribution. One way to characterize this width is through the polydispersity factor $P = s_2/s_1$,[33] where

$$s_p = \sum_{i=1}^{N_c(t)} N^p n(N) / \sum_{i=1}^{N_c(t)} N^{p-1} n(N) \qquad (9)$$

and N is the number of monomers per cluster. For a monodisperse size distribution (for instance, the HM) $P = 1$. All aggregation classes produce polydisperse size distributions with P being largest for RLCA and smallest for DLCA (Table 1). Both the OLMC model and the HM give approximately the same mass fractal dimension but clearly differ in their polydispersity. Could this be the cause of their slight difference in shape anisotropy? Previous work has eluded to polydispersity playing a role in cluster shape, but no direct measurement was performed.[35]

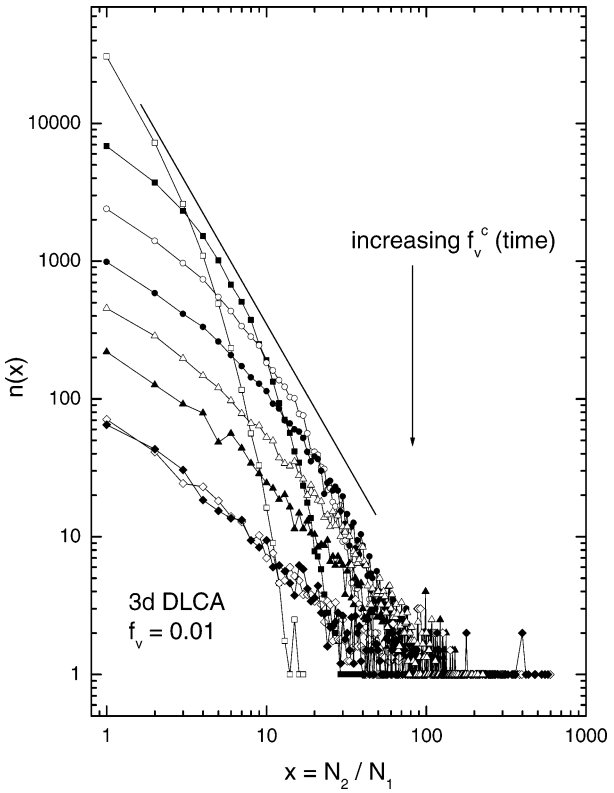

Figure 7. Histogram of the binary collision events between clusters, of size N_1 and N_2 monomers per cluster, for the DLCA model. The direction of increasing time is designated in the figure. The histogram clearly shows that aggregation between equal sized clusters is not the *only* aggregation route, as assumed in simplified models. It is also interesting to note that the common tangent for the first three curves has a slope of $\simeq -2$, in accord with predictions of the scaling of the size distribution[39,40]. The solid line is drawn with a slope of -2 to guide the eye.

To try to answer this, we contrast the shape anisotropy of the OLMC model and the HM clusters by including in Table 1 results for the shape anisotropy of three variations of particle−cluster aggregation (PCA): (1) diffusion-limited aggregation (DLA), (2) ballistic-limited aggregation (BLA), and (3) reaction-limited aggregation (RLA). Clusters of up to $N = 10\,000$ in size were grown off-lattice, and the anisotropy was calculated at the addition of every $\delta N = 50$. This was averaged over 20 independent runs. The shape anisotropy reached a large N asymptote at approximately $N = 4500$. The results show that PCA clusters are rather spherical in shape ($A_{ij} \simeq 1$), as found in a previous simulation study.[36] Note also that they are more compact, as reflected by their relatively large fractal dimension, D_f, also listed in Table 1. The PCA model represents (in the limit $N \rightarrow \infty$) the limit of infinite polydispersity between two colliding clusters, i.e., a monomer of size $N = 1$ and an infinite size cluster.

Considering all three models, polydispersity increases from the HM limit at $P = 1$ to the PCA limit at $P = \infty$. The OLMC polydispersity (Table 1) is between the two but closer in value to that of the HM. Comparing shape anisotropy results for the HM, OLMC model, and PCA model (Table 1), it appears that there is some degree of correlation between polydispersity and cluster shape; that is, increasing polydispersity lowers the shape anisotropy.

(32) Robinson, D. J.; Earnshaw, J. C. *Phys. Rev. Lett.* **1993**, *71*, 715.
(33) Oh, C.; Sorensen, C. M. *J. Aerosol Sci.* **1997**, *28*, 937.
(34) Oliver, B. J.; Sorensen, C. M. *Phys. Rev. A* **1990**, *41*, 2093.
(35) *Kinetics of Aggregation and Gelation*; Family, F., Landau, D., Eds.; Elsevier Science Publishers B.V.: Amsterdam, The Netherlands, 1984.
(36) Garik, P. *Phys. Rev. A* **1985**, *32*, 1275.

Table 2. Comparison of the 2d DLCA Simulation Results and Experiments of Ref 18[a]

	simulation		
	OLMC	HM[b]	experiment
D_f	1.44 ± 0.2	1.42 ± 0.2	1.45 ± 0.1
$\langle A_{12}\rangle$	6.26 ± 0.3	7.64 ± 0.3	6.10 ± 1.3

[a] $\langle A_{ij}\rangle$ is defined according to eq 4. [b] From our 2d HM simulations.

This is not conclusive evidence. It does suggests, however, that aggregation between equal sized clusters is a simplification that sets the HM apart from our off-lattice Monte Carlo method and may be the cause of the slightly differing shape anisotropies in the two models.

4.1.2. Comparison with Experiment in 2d. The only experimental result of shape anisotropy in real systems that exists in the literature is for 2d aggregation: Robinson et al. have experimentally determined cluster anisotropy for polystyrene latex spheres undergoing dilute-limit aggregation at an air−liquid interface.[18] They controlled the aggregation kinetics by varying the molarity of salt added to the solution containing dispersed particles. Low molarity corresponded to RLCA type behavior, and high molarity corresponded to that of DLCA. Pictures of 2d aggregates were then digitized, the principle radii of gyration were calculated for an ensemble of clusters, and $\langle A_{ij}\rangle$ was defined in accordance with eq 4. To compare with this experiment, we have performed 2d dilute-limit DLCA simulations at $f_v = 0.01$. We compare (Table 2) our 2d simulation results with their experimentally determined value for the largest molarity measured, where aggregation is expected to be most similar to pure DLCA. The agreement between the OLMC results and experiment is quite good. The OLMC model appears to better represent real cluster shape in 2d than the HM; however, the HM results are within the (large) experimental error bars.

Comparison of the 2d results with 3d results shows that 2d aggregates have a greater dilute-limit anisotropy as measured in terms of the largest $\langle A_{ij}\rangle$ ratio. One might expect this trend as with increasing degrees of freedom in higher dimensions, there are more chances for the voids between branches of the tenuous structure to be filled. Indeed, this is the case for unrestricted random walks and both linear and ring polymers.[37,38]

4.2. Comment on Anisotropy When Dense. We find that both measures of shape anisotropy decrease at large cluster volume fractions. Further aggregation drives a continuous decrease in anisotropy. This is most pronounced in the DLCA model, with RLCA showing less change. Once the system gels, the anisotropy appears to reach, within the rather large scatter, a smaller value somewhat independent of the aggregation class. We comment here on possible explanations for this change when dense.

It is not a priori clear how shape depends on cluster size. One might expect that, when dilute, because the clusters are self-similar, shape may also be self-similar. On the other hand, large clusters may grow at the expense of small clusters and become less anisotropic. This would then show up as a size dependent cluster shape. We have checked this explicitly by histogramming the largest anisotropy ratio, A_{13}, as a function of the number of monomers per cluster, N. As shown in Figure 8, at both small f_v^c values (early times) and large f_v^c values (late times), cluster shape is, within the error bars, relatively independent of N. There is a small, systematic decrease

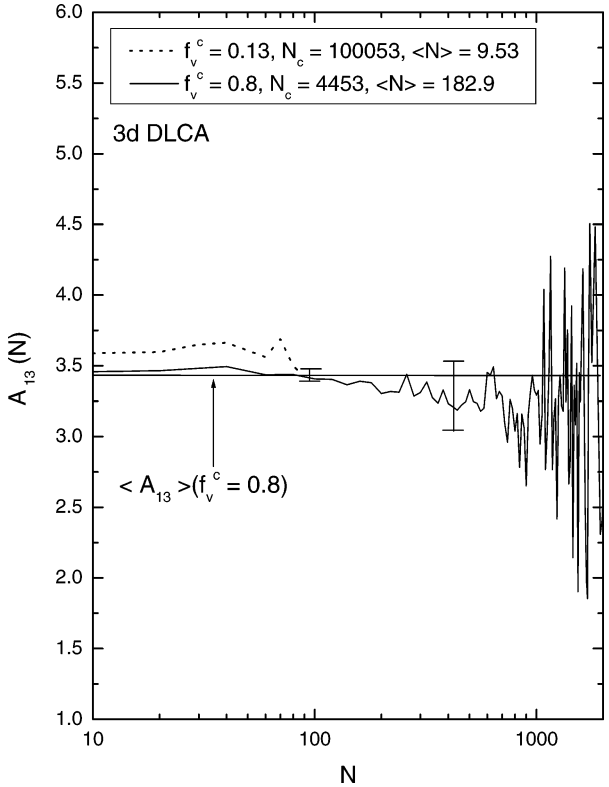

Figure 8. Dependence of A_{13} on the cluster size, N. The monomer volume fraction is $f_v = 0.01$. The solid horizontal line is drawn at the value of $\langle A_{13}\rangle$ at $f_v^c = 0.8$.

in shape for $f_v^c = 0.8$ and $N > 200$, which may be interpreted as a weak size dependence. We also show, in Figure 8, $\langle A_{13}\rangle$ at $f_v^c = 0.8$ (solid horizontal line). The fact that large clusters become less anisotropic may indicate that clusters which are larger than some correlation length are less anisotropic, and this may lead to a decrease of the overall anisotropy as the system becomes dense and ultimately reaches the gel point. We also note however that, near the gel limit, polydispersity in cluster size diverges. As we have already pointed out (see section 4.1.1), an increase in polydispersity also tends to decrease the mean anisotropy. This may also contribute to the decrease in shape anisotropy when dense.

We have observed[4,41] (see also refs 42 and 43) in recent DLCA simulations that fractal aggregates with the dimension $D_f = 1.8$ grow to fill the entire volume whereupon they percolate to superaggregates with $D_f = 2.6$, which is also the fractal dimension of random (site, bond, or continuum) percolation clusters. The crossover length scale between $D_f = 1.8$ and $D_f = 2.6$ morphologies in the superaggregate is the ideal gel point size (see eq 8). Thus, a connection of the change of shape anisotropy to percolation would seem reasonable. Further support of this connection is that the DLCA shape begins to evolve roughly when $f_v^c \simeq 0.3 \pm 0.1$, intriguingly close to various 3d percolation thresholds.

Although appealing, caution must be used when making this analogy. To begin with, the "backbone" will contribute little to the ensemble averaged anisotropy, that is, $\langle A_{ij}\rangle$.

(37) Rudnick, J.; Gaspari, G. *J. Phys. A* **1986**, *19*, L191−L193.
(38) Bishop, M.; Saltiel, C. *J. Chem. Phys.* **1986**, *85*, 6728.
(39) Meakin, P.; Vicsek, T.; Family, F. *Phys. Rev. B* **1985**, *31*, 564.
(40) Within mean-field theory, the probability that two clusters of sizes i and j aggregate is $P_i(j) = K(i, j)\, n(j)$, where $K(i, j)$ is the aggregation kernel and $n(j)$ is the cluster size distribution.
(41) Fry, D.; Chakrabarti, A.; Kim, W.; Sorensen, C. M. *Phys. Rev. E* **2004**, *69*, 061401.
(42) Gimel, J. C.; Durand, D.; Nicolai, T. *Phys. Rev. B* **1995**, *51*, 11348.
(43) Hasmy, A.; Jullien, R. *Phys. Rev. E* **1996**, *53*, 1798.

Likewise, the fractal nature of the clusters admits a certain degree of ambiguity in the definition of f_v^c. The anisotropic cluster shape[44] and the variance in cluster size add a further complexity that makes a comparison to percolation theory difficult. We show for comparison however in Figures 1−4 the location of the known percolation threshold, represented by the shaded region, for site percolation on cubic, triangular, face-centered cubic (fcc), and body-centered cubic (bcc) lattices, 3d continuum percolation,[45] and the results of Garboczi et al.[44] for percolating ellipsoids of revolution (at the same aspect ratio c/a as we find for the dilute-limit OLMC model). To compare percolation and the OLMC model, one must look at the OLMC model in the vicinity of the first system-spanning cluster. This point is designated in Figures 1−4 by the vertical arrows. In Figures 1−4, we have also added for comparison the shape anisotropy for site percolation simulations for lattice sizes up to $L = 256$ at the percolation threshold. The site percolation results compare reasonably well with the measured shape anisotropies at the gel limit.

5. Concluding Remarks

We have performed large-scale off-lattice Monte Carlo simulations to investigate aggregate shape for systems which undergo irreversible aggregation with monomer volume fractions of $f_v = 0.001$, 0.005, 0.01, and 0.1. When dilute, aggregate shape anisotropy is different for each of the three aggregation classes and is slightly different than that of the hierarchial model. As the system evolves, the shape anisotropy is constant until it becomes dense. Within each aggregation class, all measures of anisotropy presented are independent of the monomer volume fraction, f_v, when plotted as a function of the cluster volume fraction, f_v^c. This independence of f_v implies that not only is f_v^c a universal descriptor of aggregation kinetics[24] but it may also be treated as a *universal descriptor of aggregate shape*. The distribution of shape anisotropy is asymmetric, extending out to values as large as ∼15 for the ratio of the largest-to-smallest principle radii of gyration. At large A_{ij}, the distribution appears exponential with a decay constant that systematically increases from DLCA to BLCA and RLCA. A full understanding of the distribution could be of large importance in understanding the flow properties of particulate dispersions where aggregation is allowed.

As a final note, we remark that more experimental work is needed on aggregate shape, specifically in 3d. Future experiments on depolarized light scattering from fractal aggregates will provide for a better comparison with our models.[46]

Acknowledgment. Financial support was given by NASA Grant No. NAG 3-2360.

Appendix

The moment of inertia tensor, $\mathbf{T}_I$, in 3d for a body composed of N discrete point masses of unit mass is

$$\mathbf{T}_I = \sum_{l=1}^{N} \begin{pmatrix} y_l^2 + z_l^2 & -x_l y_l & -x_l z_l \\ -x_l y_l & x_l^2 + z_l^2 & -y_l z_l \\ -x_l z_l & -y_l z_l & x_l^2 + y_l^2 \end{pmatrix} \tag{10}$$

The moment of inertia tensor, $\mathbf{T}_I$, is just one of several ways of quantifying departure from spherical symmetry.[11,26,37] The frequently used "radius of gyration" tensor, $\mathbf{T}_R$, in 3d for a body composed of N discrete point masses is

$$\mathbf{T}_R = \frac{1}{N} \sum_{l=1}^{N} \begin{pmatrix} x_l^2 & x_l y_l & x_l z_l \\ x_l y_l & y_l^2 & y_l z_l \\ x_l z_l & y_l z_l & z_l^2 \end{pmatrix} \tag{11}$$

There have been numerous works addressing the symmetry of unrestricted and self-avoiding random walks as well as the shapes of ring polymers using eq 11.[37,38,47,48] There is an important difference between the tensor components and the corresponding eigenvalues. For direct comparison, we now define $\tilde{\mathbf{T}}_I = (1/N)\mathbf{T}_I$ as the corresponding radius of gyration tensor associated with the inertia tensor. By the very nature of the term "gyration", the principle radii of gyration are defined as the radii, in a plane perpendicular to a given rotation axis at which all of the mass of a body could be located, to have the same moment of inertia about that axis. The principle radii of gyration from diagonalizing $\tilde{\mathbf{T}}_I$ are perpendicular to one of the d mutually orthogonal rotation axes. Those given by $\mathbf{T}_R$ represent a characteristic linear cluster size along a rotation axis. Both of these tensors are symmetric. Furthermore, the trace of each is invariant and related to the overall size of the body as

$$\mathrm{Tr}(\tilde{\mathbf{T}}_I) = 2R_g^2 \tag{12}$$

$$\mathrm{Tr}(\mathbf{T}_R) = R_g^2 \tag{13}$$

where R_g is the spherically averaged radius of gyration (eq 1). Summing $\tilde{\mathbf{T}}_I$ and $\mathbf{T}_R$,

$$\tilde{\mathbf{T}}_I + \mathbf{T}_R = R_g^2 \mathbf{I} \tag{14}$$

where $\mathbf{I}$ is the identity matrix. Because the sum is a constant, $\tilde{\mathbf{T}}_I$ and $\mathbf{T}_R$ cannot be independent of one another. Properly choosing the matrix $\mathbf{S}$ to diagonalize $\tilde{\mathbf{T}}_I$ results in

$$\mathbf{S}^{-1}\tilde{\mathbf{T}}_I\mathbf{S} + \mathbf{S}^{-1}\mathbf{T}_R\mathbf{S} = R_g^2\mathbf{I} \tag{15}$$

Rearranging terms shows that this same transformation with $\mathbf{S}$ also diagonalizes $\mathbf{T}_R$ and relates its eigenvalues, or squares of principle radii, λ_i values, to those of $\tilde{\mathbf{T}}_I$ as

$$\lambda_i = R_g^2 - R_i^2 \tag{16}$$

Recall from section 2 that another measure of shape anisotropy can be obtained from $\tilde{\mathbf{T}}_I$ by constructing an equivalent inertia ellipsoid with axes d_i (eq 6). Using eq 12,

$$d_i^2 = \frac{4}{5}(R_g^2 + R_i^2) \tag{17}$$

Taking ratios of the squares of largest-to-smallest axes,

$$\frac{d_i^2}{d_j^2} = \frac{(R_g^2 - R_i^2)}{(R_g^2 - R_j^2)} \tag{18}$$

This result shows that, interestingly, $\mathbf{T}_R$ is actually the

(44) Garboczi, E. J.; Snyder, K. A.; Douglas, J. F.; Thorpe, M. F. *Phys. Rev. E* **1995**, *52*, 819.
(45) Stauffer, D.; Aharony, A. *Introduction to Percolation Theory*; Taylor & Francis: London, 1985.
(46) Lu, N.; Sorensen, C. M. *Phys. Rev. E* **1994**, *50*, 3109.
(47) Bishop, M.; Michels, J. P. J. *J. Chem. Phys.* **1985**, *83*, 4791.
(48) Bishop, M.; Michels, J. P. J. *J. Chem. Phys.* **1986**, *85*, 5961.

tensor associated with the equivalent inertia ellipsoid. The diagonal elements of $\mathbf{T}_R$ are the mean square distance along each of the d mutually perpendicular axes. Because the equivalent ellipsoid assumes a uniform mass distribution, not valid for tenuous aggregates, we contend that it should be used as a descriptor of shape with discretion. Further inspection of $\tilde{\mathbf{T}}_I$ and $\mathbf{T}_R$ shows that the two tensors are quite similar in 2d. Indeed, we find from simulation that in 2d the two measures give approximately the same result.

LA0494369